Supplementary Information (SI) for Journal of Materials Chemistry A.

Supporting Information

Flexible Self-Supporting CoNi Alloy-Doped Carbon Nanofibers with Uniformly Dispersed Nanoparticles: A 3D Host for Stable Lithium Metal Anode

*Yichen Cao[1], Lantao Liu[2], Hongxing Wang[1], Yiming Li[1], Zhigang Zhang[1], Zhaoping Song[1], Changchang Liu[1], Xiaoyu Xu[1], Huaihe Song[1] and Xiaohong Chen[1, *]*

1 State Key Laboratory of Chemical Resource Engineering, Beijing Key Laboratory of Electrochemical Process and Technology for Materials, Beijing University of Chemical Technology, Beijing 100029, P.R. China.

2 Petrochemical Research Institute, PetroChina Company Limited,102206 Beijing, P. R. China.

Corresponding Author

Xiaohong Chen: chenxh@mail.buct.edu.cn

Author Contributions

The manuscript was written through contributions of all authors. All authors have given approval to the final version of the manuscript.

Notes

The authors declare no competing financial interest.

Acknowledgements

This work was supported by the National Natural Science Foundation of China (52372039).

Experimental Section

Synthesis of samples: Typically, 10 wt % of polyacrylonitrile (PAN, Mw = 150 000, Macklin) was dissolved in 20 mL of N,N-dimethylformamide (DMF, 99.9%, Aladdin). Subsequently, 1 mmol of $Co(NO_3)_2 \cdot 6H_2O$ (99.99%, Macklin) and 1 mmol of $Ni(NO_3)_2 \cdot 6H_2O$ (99.99%, Macklin) were added to the solution under continuous stirring at 50°C for 8 hours to form a homogeneous precursor. The homogeneously dispersed solution was then loaded into a 10 ml syringe, the distance from the needle to the collector was set to 10 cm, and the syringe was pushed at a rate of 1 mL h^{-1} at 15 kV. The initial fiber mat was collected after about 6 hours, pre-oxidized at 260°C for 2 h, and then carbonized in a nitrogen atmosphere at 800°C for 2 h to obtain CoNi alloy nanoparticles doped carbon nanofibers (CN-CNF). Monometallic-doped carbon nanofibers synthesized by adding 2 mmol of $Co(NO_3)_2 \cdot 6H_2O$ or $Ni(NO_3)_2 \cdot 6H_2O$ were nameed as Co-CNF and Ni-CNF. In addition, the CNF was prepared without additive using the same process. Additional samples were prepared using 0.67 mmol of $Co(NO_3)_2 \cdot 6H_2O$ and 1.33 mmol of $Ni(NO_3)_2 \cdot 6H_2O$ (for CN12-CNF), and 1.33 mmol of $Co(NO_3)_2 \cdot 6H_2O$ and 0.67 mmol of $Ni(NO_3)_2 \cdot 6H_2O$ (for CN21-CNF), while keeping the total metal and PAN content constant. Similarly, CN0.5-CNF and CN2-CNF were synthesized with 0.5 mmol and 2 mmol of both $Co(NO_3)_2 \cdot 6H_2O$ and $Ni(NO_3)_2 \cdot 6H_2O$ (1:1 molar ratio), respectively, following the same electrospinning and thermal treatment procedures.

Material Characterization: SEM (Zeiss Supra 55), HRTEM (Tecnai G2 F30), and element mapping (attached to the HRTEM) were used to determine sample morphology. X-ray diffraction (XRD)(Ultima IV) was used to identify crystalline phases. The Raman spectrometer (Aramis, Jobin Yvon, with 532 nm laser excitation source) was used to evaluate the defect density of the carbon matrix. Surface elemental composition and chemical states were analyzed via X-Ray Photoelectron Spectroscopy (XPS)(Thermo VG ESCALAB 250). Using Brunauer-Emmett-Teller (BET)(ASAP2020) analysis to determine specific surface area and pore size distribution. The Inductively Coupled Plasma Optical Emission Spectrometer (ICP-OES)(Optima 5300 DV) was used to analyze the elemental content of samples.

Electrochemical Characterization: All the lithium mental cells utilizing a separator (Celgard 2500) in coin cells (CR2032) were assembled in a glovebox filled with pure argon. As the electrolyte for each cell, 1 M lithium bis (trifluoromethane) sulfonamide (LiTFSI) was dissolved in 1,3-dioxolane (DOL) and 1,2-dimethoxyethane (DME) in a volume ratio of 1:1 and 5 wt% $LiNO_3$ was added as an additive. CNF, Co-CNF, Ni-CNF and CN-CNF samples were directly used as working electrodes in half-cells, while lithium metal foils were used as counter electrodes for CE and charge/discharge experiments. Lithium was deposited on the anode of four electrodes at 1 mA cm^{-2} for 6 mAh cm^{-2} as the anode and cathode of the symmetric cell. In the full cell, LFP electrode was used as the cathode and the anode was the same as that of the symmetric cell. LFP electrodes (loading of 4–5 mg cm^{-2}) were prepared from $LiFePO_4$, poly(1,1-difluoroethylene) (PVDF), and Super P in N-methylpyrrolidone at a mass ratio of 8:1:1, coated on aluminum foils, and dried at 120 °C for 12 h. The galvanostatic charge-discharge (GCD) and cyclic voltammetry (CV) were studied on CT2001A test instrument (Wuhan LAND) and CHI 760 E electrochemical workstation (Shanghai Chenhua), respectively. The electrochemical impedance spectroscopy (EIS) tests were tested on electrochemical workstation in the frequency range of 0.01-100000 Hz with an amplitude of 1.2 V. For the half cells tests, the voltage window was 0.01–0.5 V. And the voltage window of full cells was 1.8–4 V.

Calculation method: All density functional theory (DFT) calculations were performed using the CASTEP module within the Materials Studio package. The exchange–correlation interactions were treated using the Perdew-Burke-Ernzerhof (PBE) functional under the generalized gradient approximation (GGA). The plane-wave cutoff energy was set to 400 eV, and a 3×3×1 Monkhorst-Pack k-point mesh was applied for Brillouin zone sampling. A vacuum spacing of 15 Å was employed along the z-direction to eliminate interlayer interactions.

To simulate the interaction between lithium atoms and different metal clusters, we constructed a single-layer 6×6×1 graphene supercell as the substrate. A central carbon ring was removed to introduce a vacancy, and an alloy or pure metal cluster was anchored at the defect site. For single-metal models (Co and Ni), we introduced metal clusters composed of 8 Co or 8 Ni atoms arranged in a unit cell. For the bimetallic system, a CoNi cluster consisting of 4 Co and 4 Ni atoms was built with random atomic distribution within the same unit cell. All clusters were placed atop the graphene substrate with full exposure to mimic practical interfaces in carbon-supported Li metal anode.

All initial configurations were fully geometry-optimized until the total energy and maximum atomic forces converged below 1.0×10^{-5} eV and 0.03 eV/Å, respectively. The adsorption behavior of a single lithium atom was then investigated by placing Li above the optimized clusters and allowing further relaxation. The Li adsorption energy (E_{ad}) was calculated using the formula: $E_{ad}=E_{total}-E_{slab}-E_{Li}$, where E_{total} is the total energy of the Li-adsorbed system, E_{slab} is the energy of the substrate (graphene with metal cluster) after relaxation, and E_{Li} is the energy of an isolated Li atom in vacuum. This computational setup enables us to evaluate the Li affinity of each metal configuration and rationalize the experimentally observed differences in lithium nucleation behavior.

Supplementary Figures

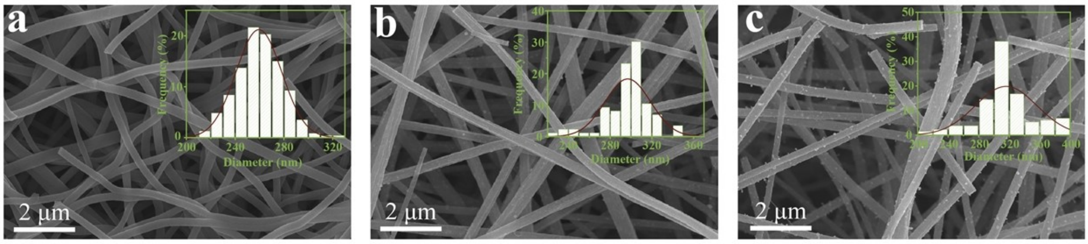

Figure S1. SEM image of (a) CNF, (b) Co-CNF and (c) Ni-CNF samples.

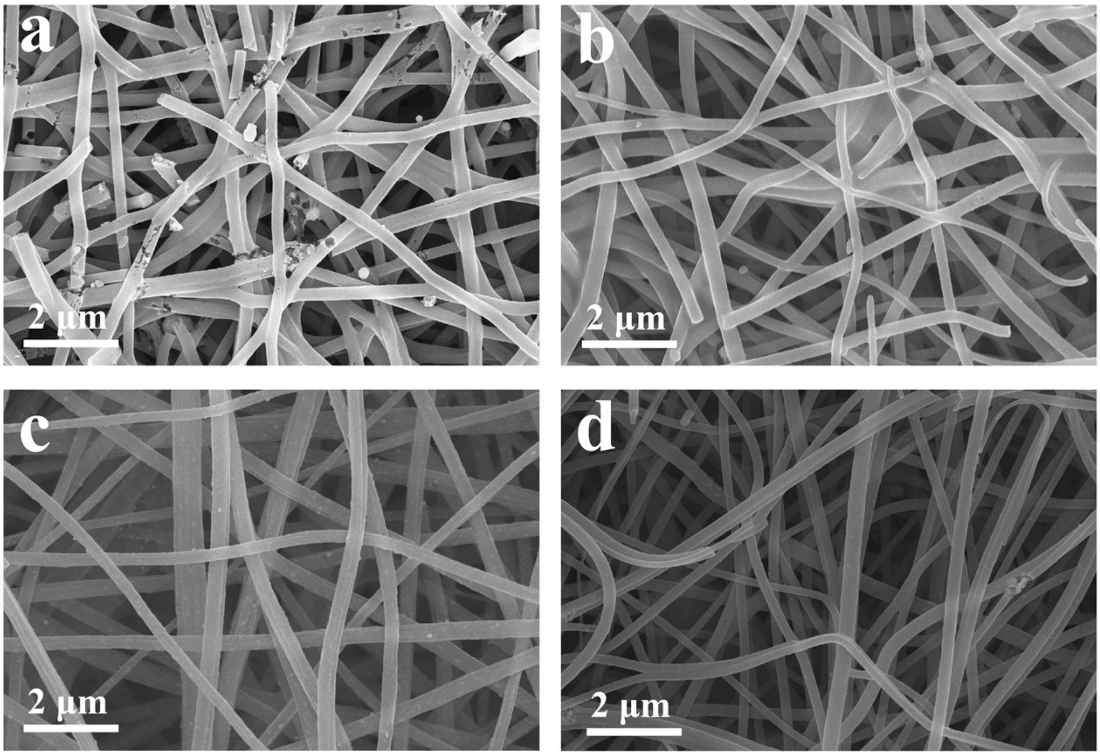

Figure S2. SEM image of (a) CN2-CNF, (b) CN0.5-CNF, (c) CN12-CNF and (d) CN21-CNF samples.

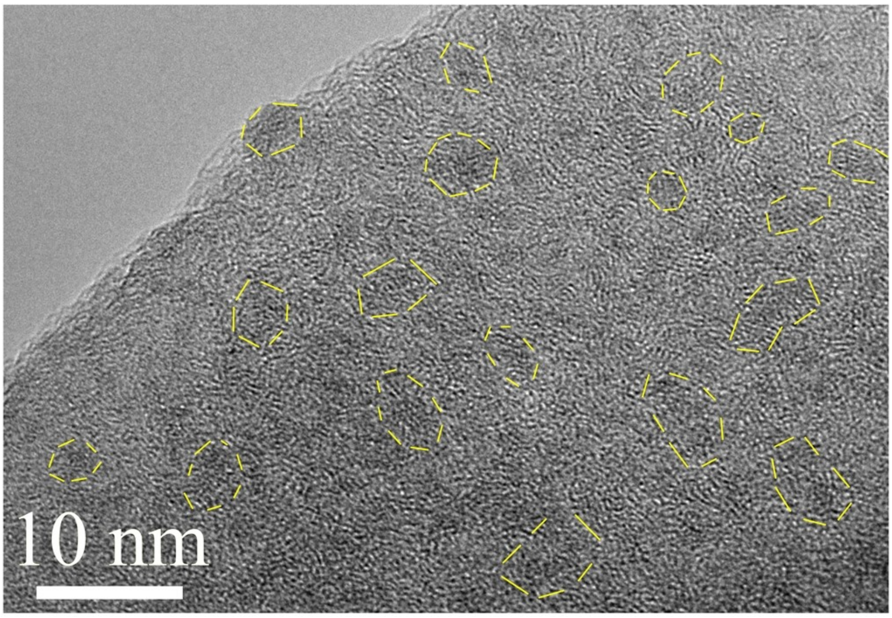

Figure S3. HRTEM image of CN-CNF.

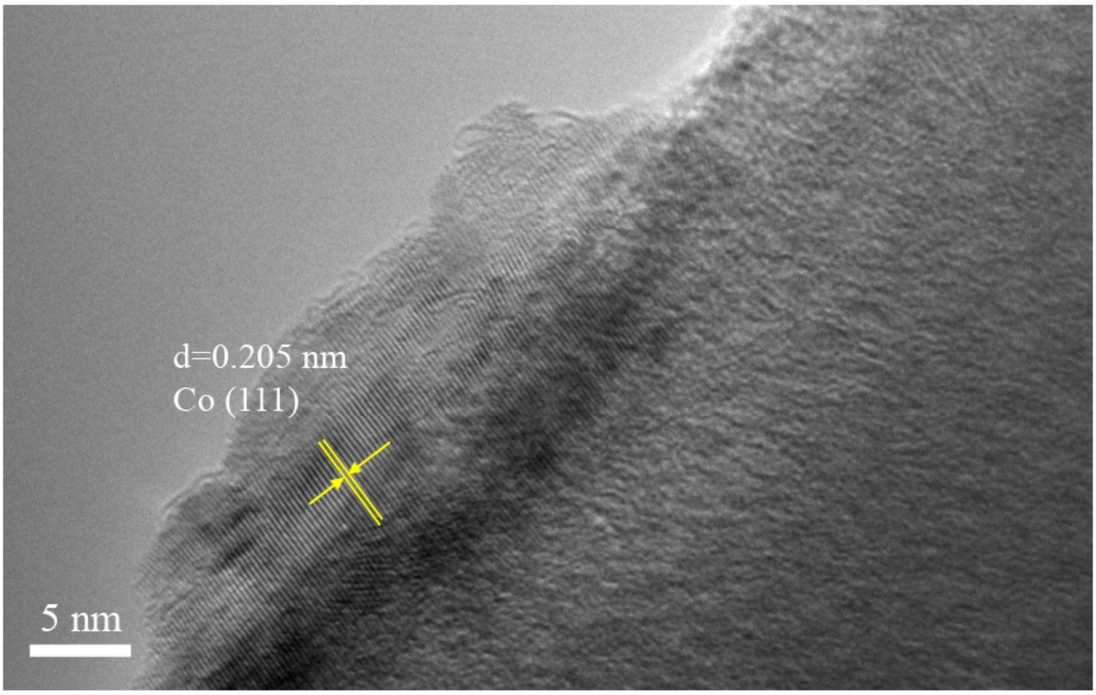

Figure S4. HRTEM image of Co-CNF.

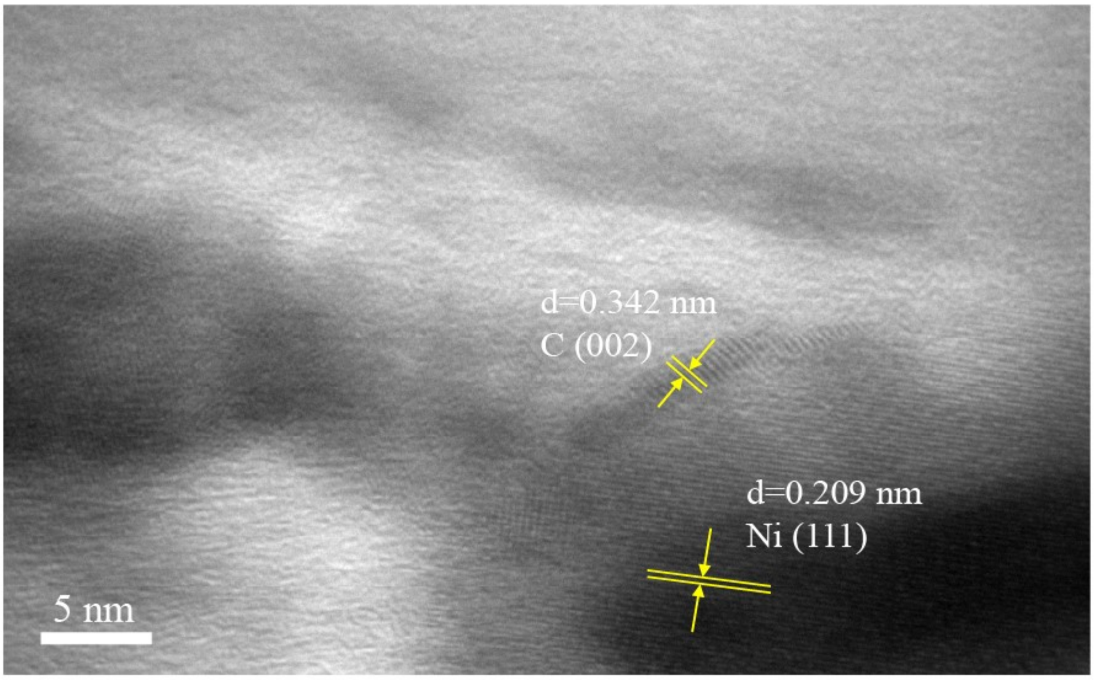

Figure S5. HRTEM image of Ni-CNF.

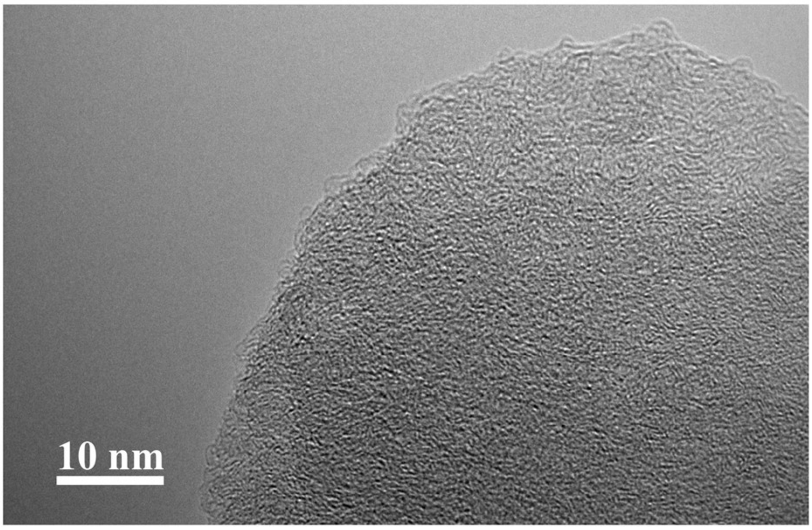

Figure S6. HRTEM image of CNF.

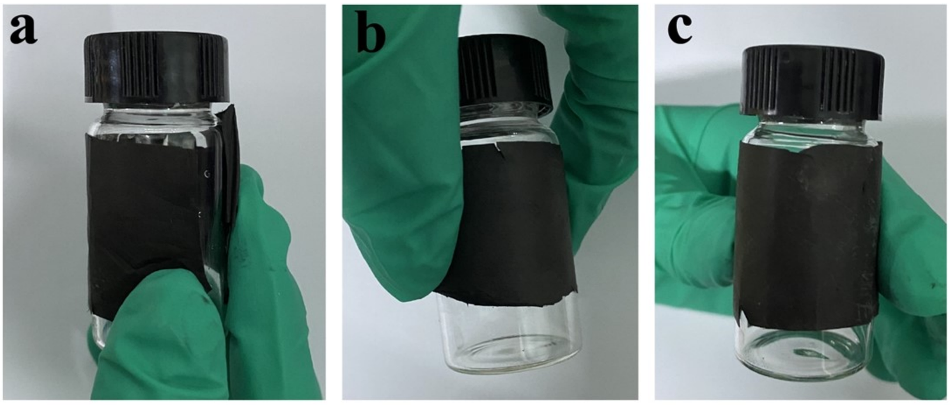

Figure S7. Photographs of (a) CNF, (b) Co-CNF and (c) Ni-CNF wrapped around the vial.

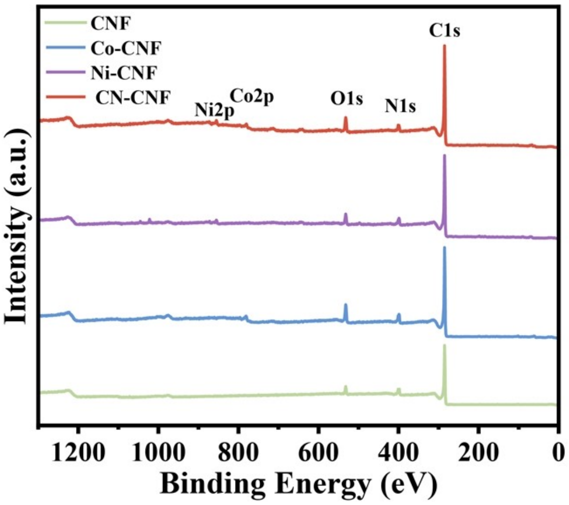

Figure S8. XPS spectra of CNF, Co-CNF, Ni-CNF and CN-CNF samples.

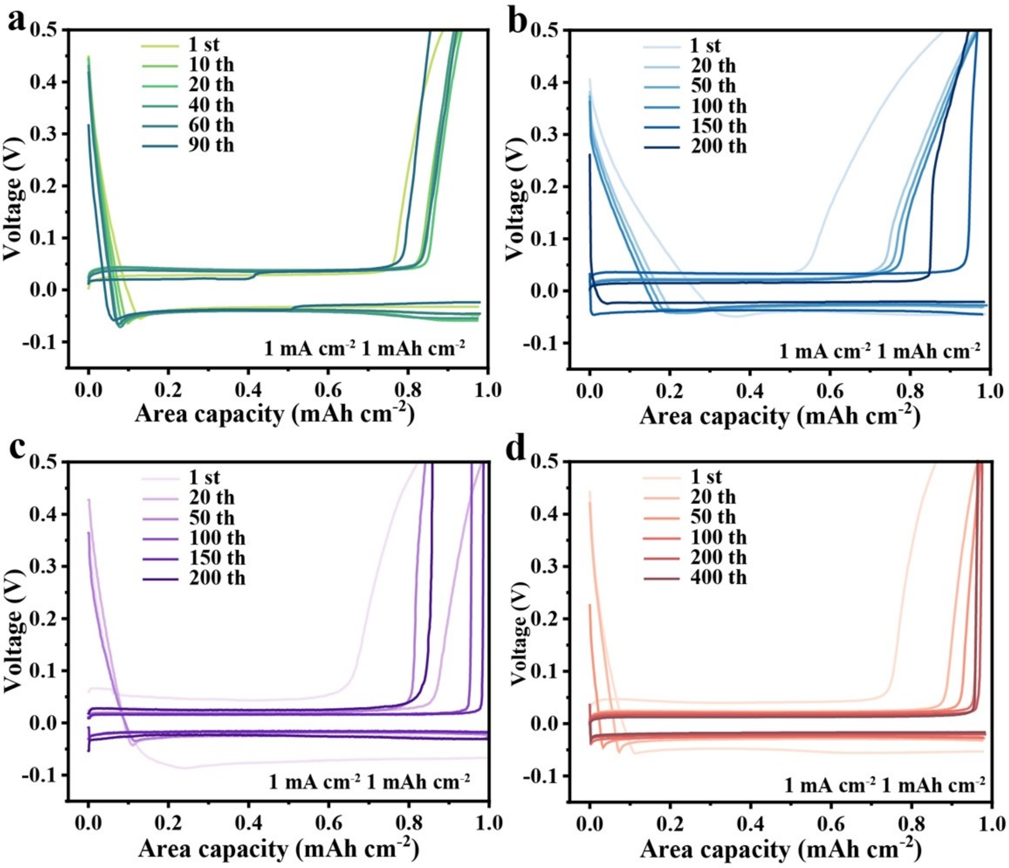

Figure S9. Voltage profiles of (a) CNF, (b) Co-CNF, (c) Ni-CNF and (d) CN-CNF at a current density of 1 mA cm^{-2} for 1 mAh cm^{-2} during different cycles.

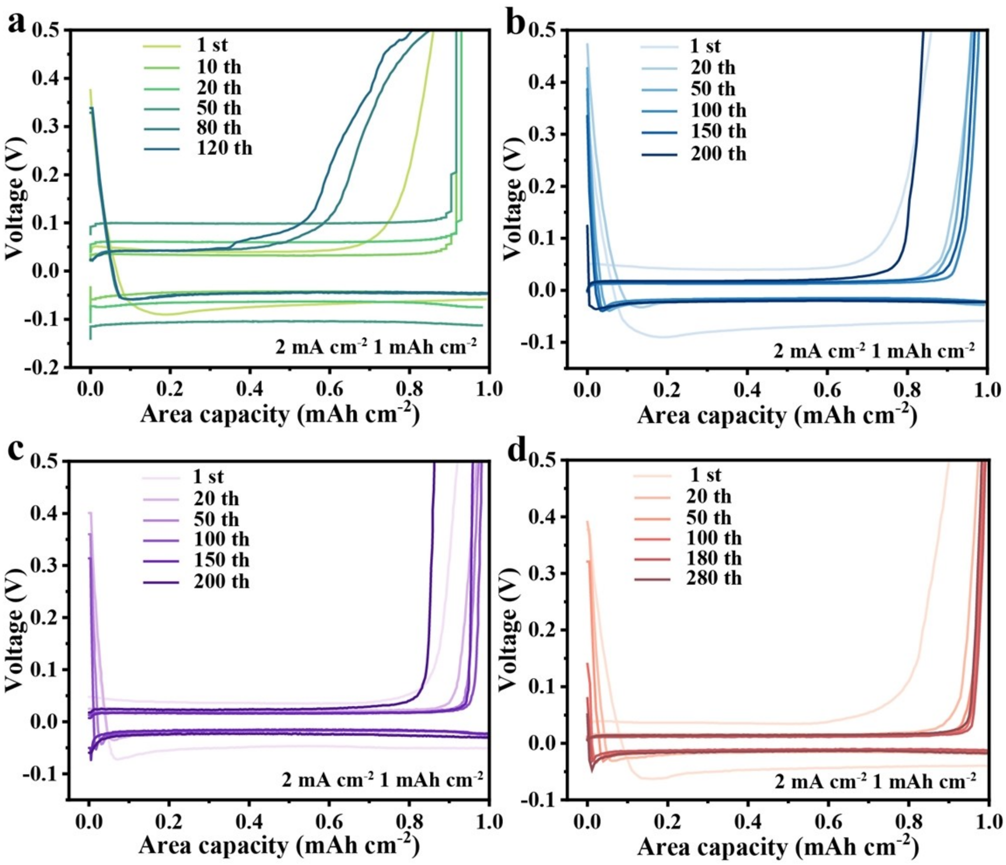

Figure S10. Voltage profiles of (a) CNF, (b) Co-CNF, (c) Ni-CNF and (d) CN-CN at a current density of 2 mA cm^{-2} for 1 mAh cm^{-2} during different cycles.

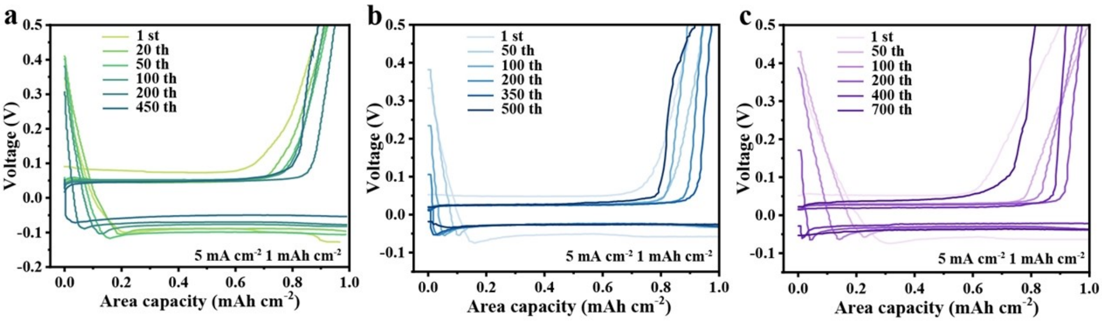

Figure S11. Voltage profiles of (a) CNF, (b) Co-CNF, (c) Ni-CNF and (d) CN-CNF at a current density of 5 mA cm^{-2} for 1 mAh cm^{-2} during different cycles.

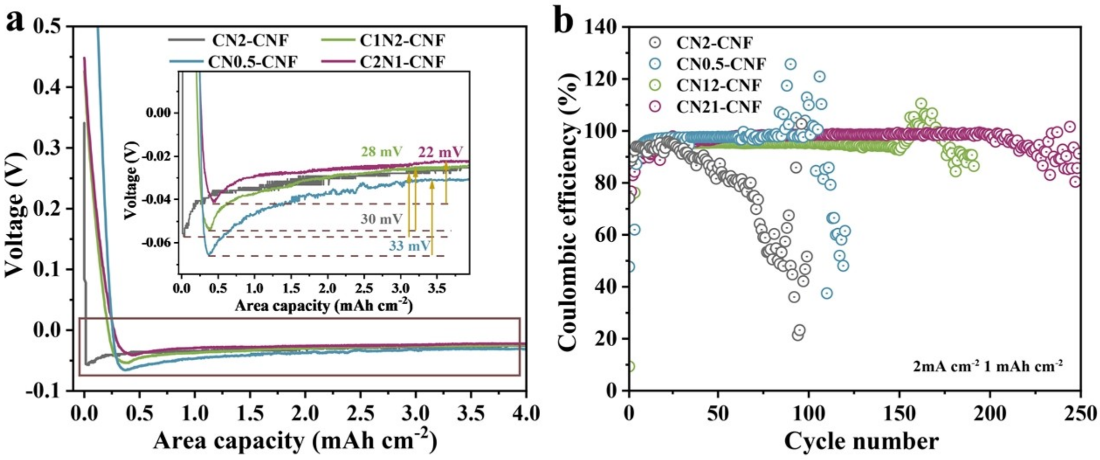

Figure S12. (a) Voltage-capacity profiles of the first lithium deposition. (b) CEs for lithium deposition/stripping of CN2-CNF, CN0.5-CNF, CN12-CNF and CN21-CNF electrodes at a current density of 2 mA cm^{-2} for 1 mAh cm^{-2}.

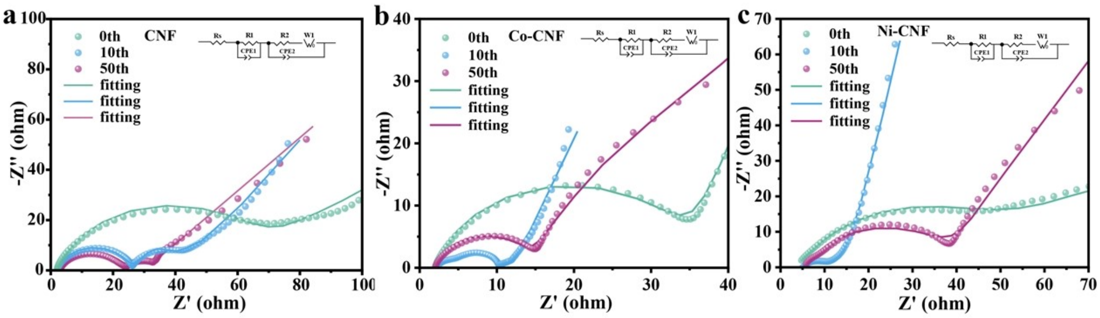

Figure S13. Measured and fitted impedance spectra of (a) CNF, (b) Co-CNF, (c) Ni-CNF electrodes during lithium deposition/stripping at different cycles.

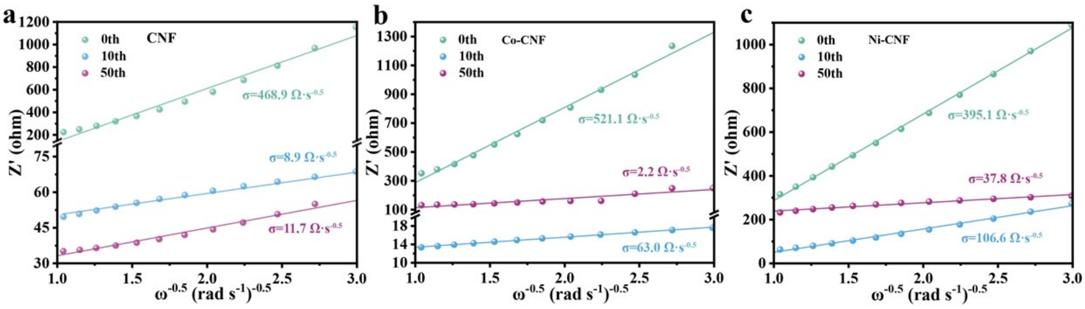

Figure S14. The relationship of (a) CNF, (b) Co-CNF, (c) Ni-CNF between the Z-Real and $\omega^{-0.5}$ at the low-frequency region.

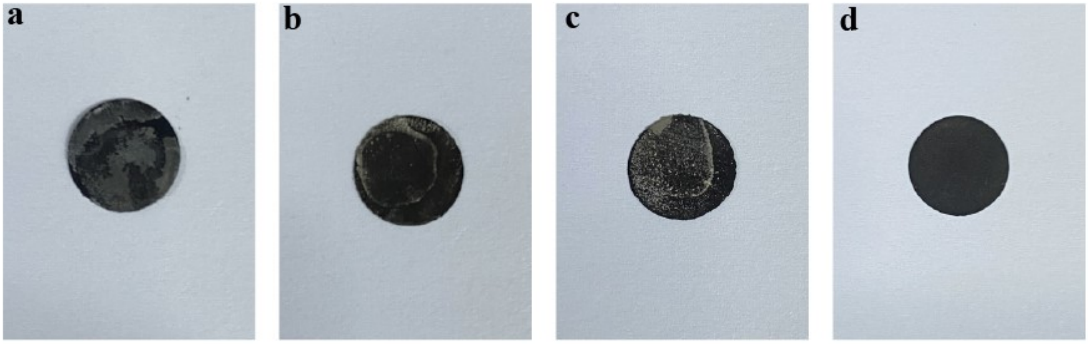

Figure S15. Macroscopic photographs of the electrode surfaces of (a) CNF, (b) Co-CNF, (c) Ni-CNF and (d) CN-CNF electrodes after 50 cycles.

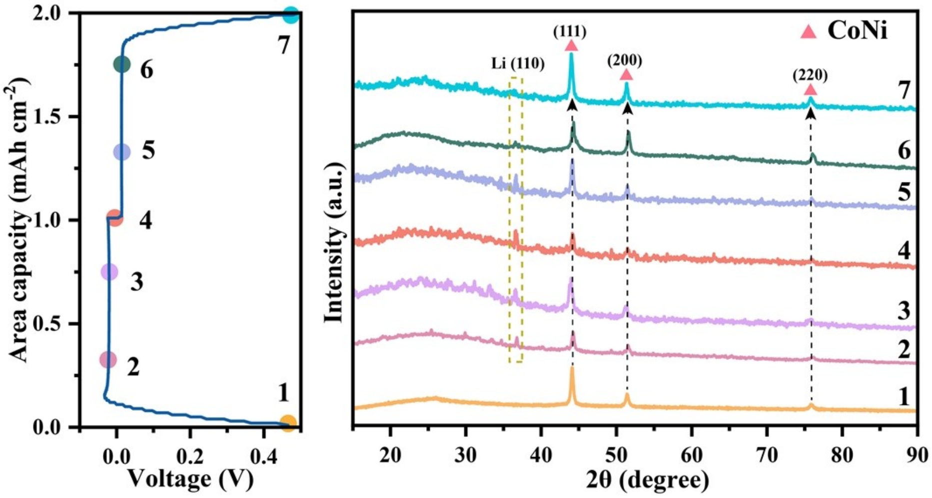

Figure S16. Ex-situ XRD patterns of CN-CNF after 10 cycles during lithium deposition/stripping at 1 mA cm^{-2} for 1mAh cm^{-2}.

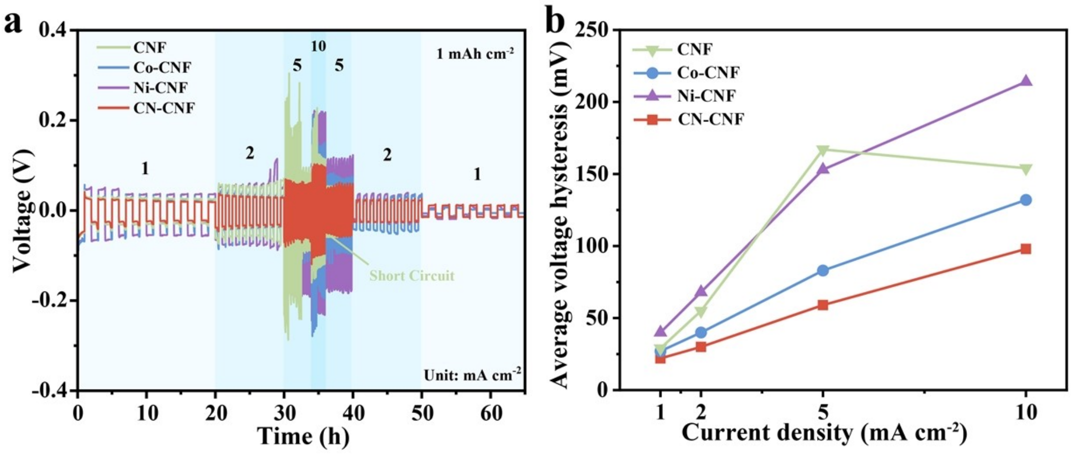

Figure S17. (a) Voltage profiles of CNF, Co-CNF, Ni-CNF and CN-CNF electrodes at different current density for 1 mAh cm^{-2} in a symmetrical cell. (b) Average voltage hysteresis of CNF, Co-CNF, Ni-CNF and CN-CNF electrodes at different current density.

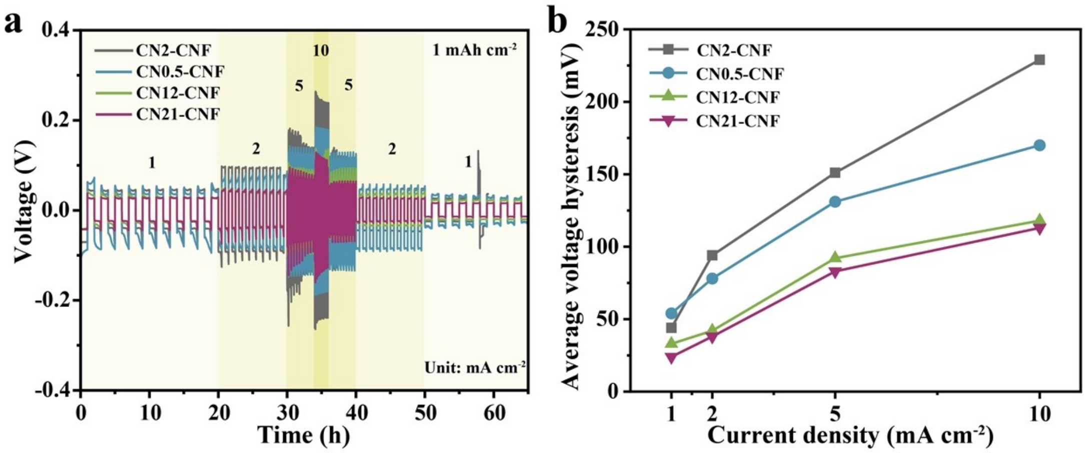

Figure S18. (a) Voltage profiles of CN2-CNF, CN0.5-CNF, CN12-CNF and CN21-CNF electrodes at different current density for 1 mAh cm^{-2} in a symmetrical cell. (b) Average voltage hysteresis of CN2-CNF, CN0.5-CNF, CN12-CNF and CN21-CNF electrodes at different current density.

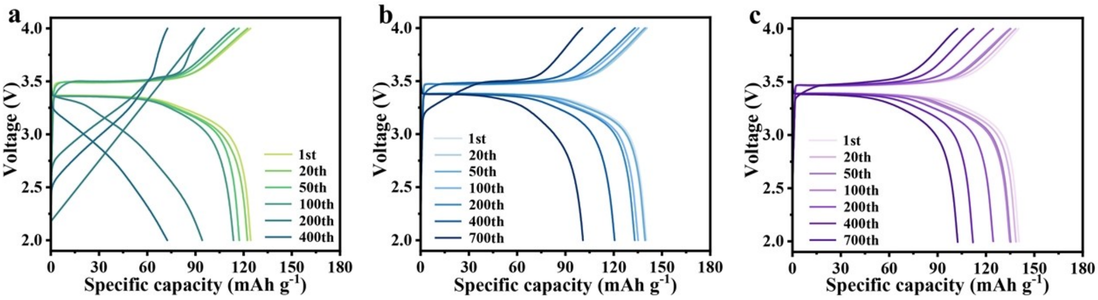

Figure S19. Voltage profiles of full cells for (a) CNF@Li, (b) Co-CNF@Li and (c) Ni-CNF@Li electrodes at 1 C with various cycles.

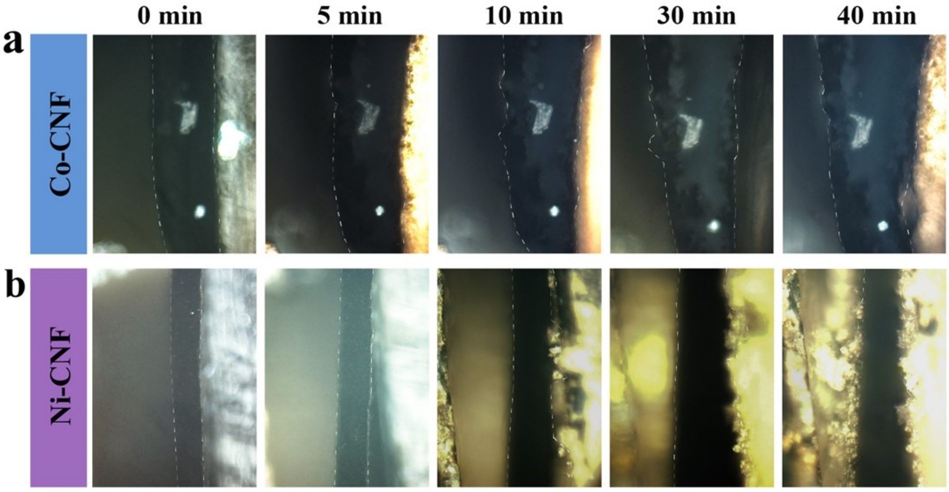

Figure S20. In situ optical microscopy images of Li deposition behavior of (a) Co-CNF and (b) Ni-CNF anodes at different deposition times.

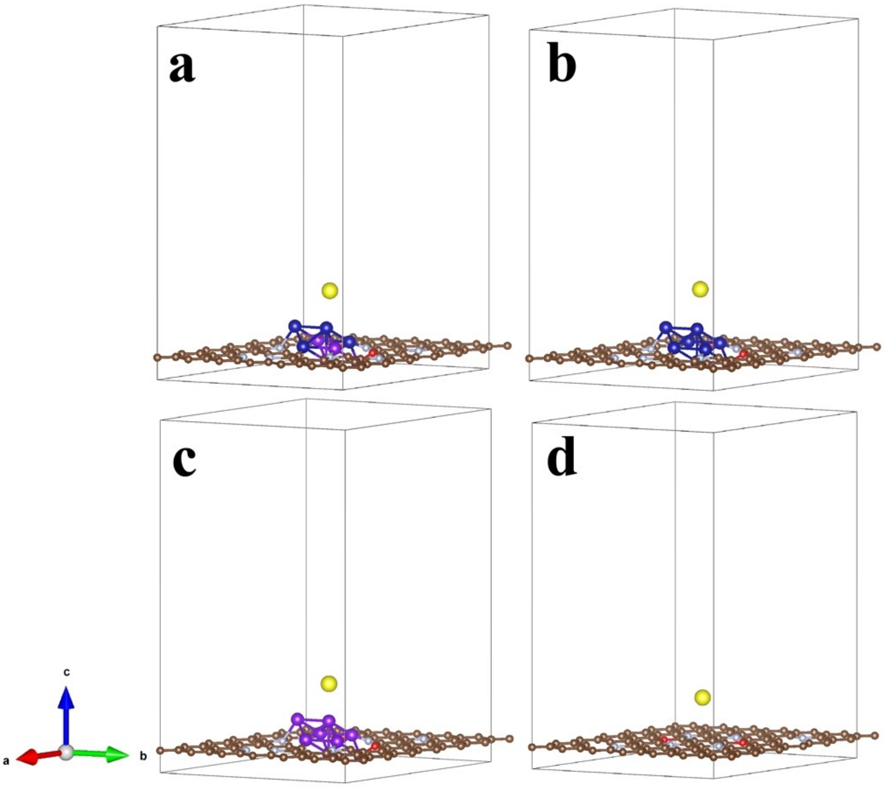

Figure S21. Adsorption models of (a) CN-CNF, (b) Co-CNF, (c) Ni-CNF and (d) CNF samples before geometry optimization.

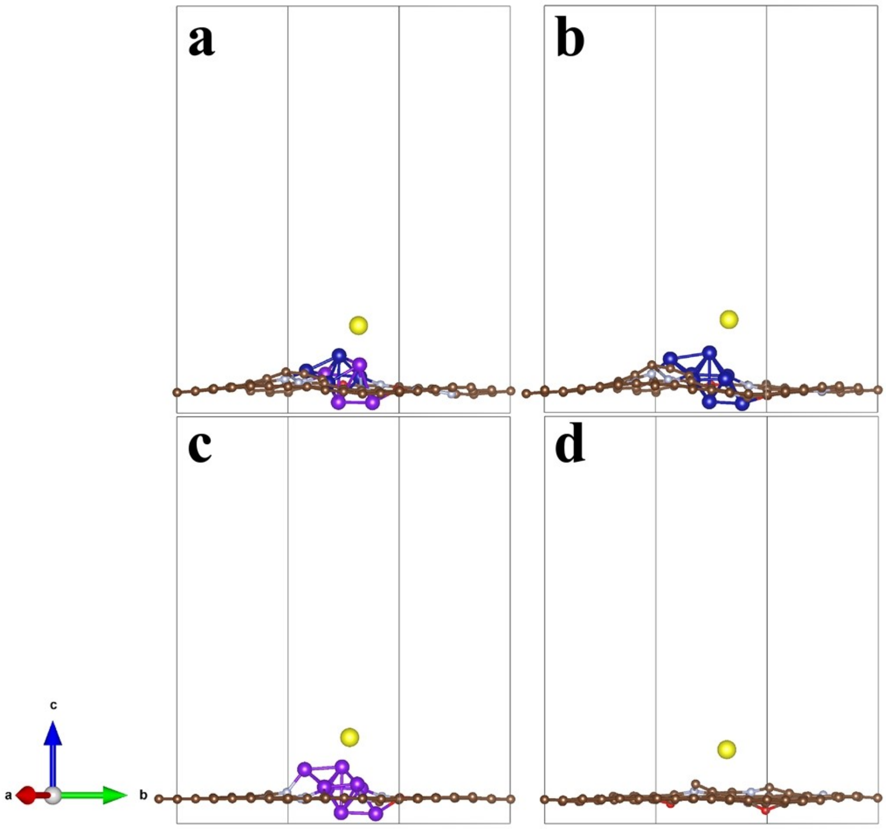

Figure S22. Adsorption models of (a) CN-CNF, (b) Co-CNF, (c) Ni-CNF and (d) CNF samples after geometry optimization.

Supplementary Figures

Table S1. The content of C, N, O, Co and Ni in four samples by ICP-OES test

Sample	C at.%	N at.%	O at.%	Co at.%	Ni at.%
CNF	85.3	7.9	6.8	0	0
Co-CNF	80.5	6.5	8.1	4.9	0
Ni-CNF	78.8	8.9	7.2	0	5.1
CN-CNF	79.9	8.7	6.5	2.7	2.2

Table S2. The content of Pyridinic-N, Pyrrolic-N, Graphitic-N, N-O and Metal-N_x in the four samples by XPS spectra

Sample	Pyridinic-N %	Pyrrolic-N %	Graphitic-N %	N-O %	Metal-N_x %
CNF	37.9	27.4	17.8	16.9	0
Co-CNF	30.6	24.1	12.4	15.6	17.3
Ni-CNF	28.9	25.8	13.1	17.9	14.3
CN-CNF	29.6	26.8	12.7	15.6	15.3

Table S3. Fitting results of EIS tests during Li deposition/stripping for CN-CNF, Co-CNF, Ni-CNF and CNF at different cycles

Sample	R_s (Ω)	R_1 (Ω)	R_2 (Ω)
CN-CNF 0th	1.6	35.7	15.8
CN-CNF 10th	2.1	4.6	11.5
CN-CNF 50th	1.9	4.3	10.7
Co-CNF 0th	2.0	32.6	17.4
Co-CNF 10th	2.5	5.8	6.3
Co-CNF 50th	2.1	11.9	29.4
Ni-CNF 0th	1.8	38.1	31.1
Ni-CNF 10th	4.5	6.3	10.6
Ni-CNF 50th	5.8	32.7	25.2
CNF 0th	2.3	62.4	48.1
CNF 10th	2.0	21.3	32.4
CNF 50th	3.2	25.6	18.6

Table S4. Comparison of electrochemical performance in symmetrical batteries

	Current density (mA cm^{-2})	Area capacity (mAh cm^{-2})	Cycle life (h)	Ref.
This work	1	1	2200	
	5	2.5	750	
	10	1	1000	
Cu_3P/CoP@C/CNT	1	1	400	[1]
NCF@$NiCo_2S_4$	1	1	1200	[2]
	3	1	350	
	10	1	85	
Laser-Constructing 3D Copper	0.5	0.5	1600	[3]
Ag@NCS	1	1	300	[4]
Cu/Cu_3P-N-CNFs	1	1	1500	[5]
Bidirectional lithiophilic gradient carbon nanofiber	1	1	600	[6]
SiO_2-Cu_2O	1	1	1000	[7]
NPCC	3	1	600	[8]
	5	1	240	
$Ti_3C_2T_x$/g-C_3N_4	0.5	1	1050	[9]
MnO@BDCNF	1	1	500	[10]

Table S5. Fitting results of EIS tests for CN-CNF@Li, Co-CNF@Li, Ni-CNF@Li and CNF@Li electrodes in full cells

Sample	R_s (Ω)	R_{ct} (Ω)
CN-CNF@Li	2.9	5.9
Co-CNF@Li	3.6	9.4
Ni-CNF@Li	4.1	13.1
CNF@Li	3.4	15.3

Reference

[1] X. Zhang, S. Jin, M. H. Seo, C. Shang, G. Zhou, X. Wang, G. Li, *Nano Energy* **2022**, 93, 106905.

[2] X. Zhang, Y. Li, H. Zhang, G. Li, *Carbon Energy* **2023**, 5, e348.

[3] H. Li, G. Wang, J. Hu, J. Li, J. Huang, S. Xu, *Energy & Environmental Materials* **2024**, 7, e12768.

[4] Z. Jiang, C. Meng, G. Chen, R. Yuan, A. Li, J. Zhou, X. Chen, H. Song, *Journal of Colloid and Interface Science* **2022**, 627, 783.

[5] Y. Xiang, L. Lu, W. Li, F. Yan, H. Wang, Z. Zhao, J. Li, A. Giri Prakash Kottapalli, Y. Pei, *Chemical Engineering Journal* **2023**, 472, 145089.

[6] T. Li, S. Gu, L. Chen, L. Zhang, X. Qin, Z. Huang, Y.-B. He, W. Lv, F. Kang, *Small* **2022**, 18, 2203273.

[7] G. Chen, Z. Li, T. Zhao, K. Wang, T. Yu, M. Feng, L. Li, F. Wu, R. Chen, *Small* **2024**, 20, 2401465.

[8] K. Li, Z. Hu, J. Ma, S. Chen, D. Mu, J. Zhang, *Advanced Materials* **2019**, 31, 1902399.

[9] F. Zhao, P. Zhai, Y. Wei, Z. Yang, Q. Chen, J. Zuo, X. Gu, Y. Gong, *Advanced Science* **2022**, 9, 2103930.

[10] X. Chen, Z. Yuan, J. He, L. Tong, Y. Wang, J. Wu, X. Li, Y. Chen, *Composites Communications* **2023**, 42, 101660.